Available online at www.sciencedirect.com
SCIENCE DIRECT®
International Journal of Mass Spectrometry 228 (2003) 743–757
International Journal of Mass Spectrometry
www.elsevier.com/locate/ijms

Ion chemistry of the hexanuclear methoxo-oxovanadium cluster $V_6O_7(OCH_3)_{12}$

Detlef Schröder[a,*], Marianne Engeser[a], Mark Brönstrup[b], Charles Daniel[c], Johann Spandl[c], Hans Hartl[c]

[a] *Institut für Chemie, Technische Universität Berlin, D-10623 Berlin, Germany*
[b] *Aventis Pharma Deutschland GmbH, Industriepark Höchst, G878, D-65926 Frankfurt/M., Germany*
[c] *Institut für Anorganische Chemie, Freie Universität Berlin, D-14195 Berlin, Germany*

Received 2 December 2002; accepted 31 March 2003

Dedicated to Professor Helmut Schwarz on the occasion of his 60th birthday.

Abstract

The hexanuclear methoxo-oxovanadium cluster $V_6O_7(OCH_3)_{12}$ (**1**) is investigated by electrospray ionization in methanol solution. Collision experiments unravel the fragmentation schemes of the molecular ions $\mathbf{1}^+$ and $\mathbf{1}^-$ as well as the H^+, Na^+, and Cs^+ adducts of **1**. In general, fragmentation of the hexanuclear cluster ions commences with sequential expulsions of two $OV(OCH_3)_3$ units to yield the corresponding V_4 clusters. However, when an active proton is present in the cluster ion, e.g., in the protonated molecule $[\mathbf{1}+H]^+$, loss of methanol precedes degradation to V_4 clusters. In addition, the experiments suggest that electrospray ionization provides as an alternative method for the generation of metal oxide cluster ions $V_mO_n{}^{+/-}$ ($m = 1$–4, $n = 0$–11).

Keywords: Electrospray ionization; Methoxo-oxovanadium cluster; Vanadium oxides

1. Introduction

Present investigations of transition metal clusters in the gas phase are by and large conducted phenomenologically in that the types of species studied are primarily determined by the ability to generate them in sufficient yields. Quite often, however, only few species in a large set of cluster ions bear particular properties (e.g., redox patterns, dissociation behaviors, reactivities). In most cases, cluster-ion generation occurs in a more or less statistical manner, where the most common approach is laser evaporation with subsequent termolecular cooling. As a consequence, only particularly stable, yet often poorly reactive clusters may evolve in good yields or—in the other extreme—broad distributions of cluster ions are produced. When it comes to heteronuclear transition metal clusters, these statistical approaches are therefore of rather ambiguous outcome as far as ion structures are concerned. Laser evaporation of vanadium in the presence of oxygen, for example, seems to afford a weakly bound dioxygen complex $V_4O_8{}^+\cdot O_2$

* Corresponding author. Tel.: +49-30-314-26546; fax: +49-30-314-21102.
E-mail address: Detlef.Schroeder@ochssrv-01-1.chem.tu-berlin.de (D. Schröder).

1387-3806/$ – see front matter © 2003 Elsevier Science B.V. All rights reserved.
doi:10.1016/S1387-3806(03)00236-7

[1], rather than the expected, and considerably more stable tetravanadium decaoxide cation $V_4O_{10}^+$ [2]; similar isomerisms in transition metal oxide clusters $M_mO_n^{+/-}$ generated by laser evaporation methods have previously been suspected by Wang and coworkers [3,4].

In this respect, inorganic synthesis offers a valuable alternative for the generation of cluster ions provided that appropriate means are available for transferring a well-defined bulk compound into the gas phase. Here, we report on the gas-phase chemistry of the hexanuclear methoxo-oxovanadium cluster $V_6O_7(OCH_3)_{12}$ (**1**), which has been prepared recently by a solvothermal methanolysis of the mononuclear vanadium(V) alkoxide $OV(Ot\text{-}C_4H_9)_3$ [5,6]. This compound and its reduced derivative $(n\text{-}C_4H_9)_4N[V_6O_7(OCH_3)_{12}]$ [6] allow a profound study of the ion chemistry of **1** in various charge states, thereby inter alia exploring an alternative approach for the generation of vanadium-oxide clusters.

2. Experimental details

The experiments were performed with a commercial VG BIO-Q mass spectrometer described elsewhere [7]. In brief, the VG BIO-Q consists of an electrospray ionization (ESI) source combined with a tandem mass spectrometer of QHQ configuration (Q stands for quadrupole and H for hexapole). In the present experiments, mmolar solutions of $V_6O_7(OCH_3)_{12}$ or $(n\text{-}C_4H_9)_4N[V_6O_7(OCH_3)_{12}]$ in methanol were introduced through a stainless steel capillary into the ESI source via a syringe pump (2–5 μL/min). Nitrogen was used as nebulizer and drying gas at source temperatures of 80–120 °C. Optimal yields of the desired cluster ions were achieved by adjusting the cone voltage (U_c) between 0 and 200 V. For collision-induced dissociation (CID) at low collision energies, the ions of interest were mass-selected using Q1, interacted with xenon as a collision gas in the hexapole H under single-collision conditions at variable collision energies (E_{lab} = 0–150 eV), while Q2 was scanned to monitor the ionic products. Likewise, *n*-butane was admitted to the hexapole in preliminary reactivity studies at E_{lab} = 0 eV, in which the pressure of the neutral substrate was raised to the multicollisional regime in some cases in order to monitor relatively inefficient reactions. In addition to pure methanol, also methanol/water (50:50), methanol/water/formic acid (50:50:1), and CD_3OD (99.5 at.% D) were used as solvents in ESI. After a few days storage at room temperature, the latter affords partial deuteration of **1** (see below); the whole sample was consumed in the measurements such that further deuteration was not examined.

As pointed out previously, the VG BIO-Q does not allow to directly extract quantitative threshold information from CID experiments due to several limitations of the commercial instrument [7]. However, the energy-dependent CID spectra show some distinct dependencies from the collision energies applied. In a strict sense, the limitations of the instrument would therefore require to display all spectra at various collision energies, if the trends evolving from comparison of energy-dependent CID spectra of different ions are to be discussed. To avoid such an exhaustive display of raw data, the threshold behaviors were analyzed in an empirical manner by fitting sigmoid functions of the type $I_i(E_{CM}) = (BR_i/1 + e^{(E_{1/2}-E_{CM})b})$ to the observed relative fragment ion yields using a least-square criterion; for the parent ion M: $I_M(E_{CM}) = \left[1 - \sum BR_i/(1 + e^{(E_{1/2,i}-E_{CM})b_i})\right]$. Here, BR_i stands for the branching ratio of a particular product ion ($\sum BR_i = 1$), $E_{1/2,i}$ is the energy at which the sigmoid function for the fragment *i* has reached half of its maximum, E_{CM} is the collision energy in the center-of-mass frame ($E_{CM} = m_T/(m_T + m_I)E_{lab}$, where m_T and m_I stand for the masses of the collision gas and the ion, respectively), and b_i describes the rise of the sigmoid curve for the fragment *i*. In consecutive dissociations, all secondary product ions were summed to the primary fragment. Further, non-negligible ion decay at E_{lab} = 0 V as well as some fraction of non-fragmenting parent ions at large collision energies (due to the single-collision conditions maintained) were acknowledged by means of scaling and normalization. This empirical, but physically reasonable approach is able to reproduce

the measured ion yields quite well. It is important to note, however, that the term $E_{1/2}$ used in the exponent does not correspond to the intrinsic appearance energies (AE) of the fragmentation of interest (see below), not to speak of the corresponding thermochemical thresholds at 0 K. The phenomenological AEs given below were derived from linear extrapolations of the rise of the sigmoid curves at $E_{1/2}$ to the base line.

With regard to the limited mass-resolving power of the VG BIO-Q, some additional high-resolution mass spectra were recorded using a commercial Bruker Apex III Fourier-transform ion-cyclotron resonance (FT-ICR) mass spectrometer (max. field strength 7 T) equipped with an external ESI source. The sample was admitted to the mass spectrometer by flow injection (ca. 1 μL/min) of a solution in methanol. The degree of fragmentation was controlled by adjusting the cone voltage (Skimmer 2 in the Apex III) between 40 and 220 V. In some experiments, fragmentation of the ions trapped in the ICR cell was enhanced by irradiation of a CO_2-laser with a power of 13 W for ca. 0.2 s prior to detection in order to induce infrared multiphoton dissociation (IRMPD). Spectra were recorded with 512 K data points, 2× zero-filled, and apodized prior to Fourier transformation. All spectra are externally calibrated. Under these conditions, the accuracy of mass determination in the range of 300–1600 amu is in the order of ±3 ppm without any further refinement.

3. Results and discussion

Schematically, the structure of **1** can be described as an octahedron of vanadium atoms with an oxygen atom in the center, a terminal oxo group at each metal atom, and 12 bridging methoxo ligands on all edges (Chart 1) [5]. According to formal electron counting, **1** contains four vanadium(IV) and two vanadium(V) centers, and thus it is a $V^{IV}_4V^{V}_2$ compound with a d^4 occupation in the valence space. Ionization changes the formal oxidation states in the molecular ions $\mathbf{1}^{-/+}$ to $V^{IV}_5V^{V}$ in the anion and $V^{IV}_3V^{V}_3$ in the cation, respectively. In the H^+, Na^+, and Cs^+ adducts of **1**, the formal oxidation state of the neutral remains unchanged.

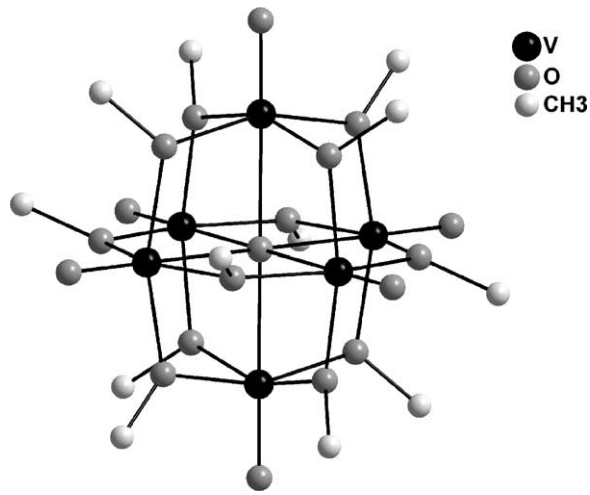

Chart 1.

3.1. Molecular ions

Fig. 1 shows the ESI mass spectrum of a solution of **1** in methanol under gentle conditions, that means a low cone voltage (here $U_c = 15$ V). From an analytical point of view, the pronounced molecular ion $\mathbf{1}^+$ with $m/z = 790$ (high resolution (HR): $m_{exp} = 789.8483$, $m_{th} = 789.8489$, $\Delta m = 0.0006$) formed under ESI conditions is quite remarkable. In fact, upon ESI of a solution of **1** in pure methanol, the ion signal at $m/z = 791$ can mostly be attributed to ^{13}C-$\mathbf{1}^+$, rather than the protonated molecule $[\mathbf{1} + H]^+$. Along with $\mathbf{1}^+$, additional signals at $m/z = 776$ and 813 are observed whose abundances depend on the ESI conditions, particularly the composition of the solvent (see below). When the cone voltage is increased, $\mathbf{1}^+$ begins to dissociate due to termolecular collisions occurring in the cone region to first afford the pentanuclear cluster $V_5O_6(OCH_3)_9{}^+$ with $m/z = 630$ ($\mathbf{2}^+$) and then the tetranuclear cluster $V_4O_5(OCH_3)_6{}^+$ with $m/z = 470$ ($\mathbf{3}^+$), corresponding to sequential losses of the neutral oxovanadium(V) alkoxide $OV(OCH_3)_3$ from the cluster cations. At further elevated cone voltages, $\mathbf{3}^+$ undergoes two competing dissociations: either expulsion of another $OV(OCH_3)_3$ unit affords the trinuclear cluster ion $V_3O_4(OCH_3)_3{}^+$ with $m/z = 310$ ($\mathbf{4}^+$) or sequential losses of outer substituents take place, mainly

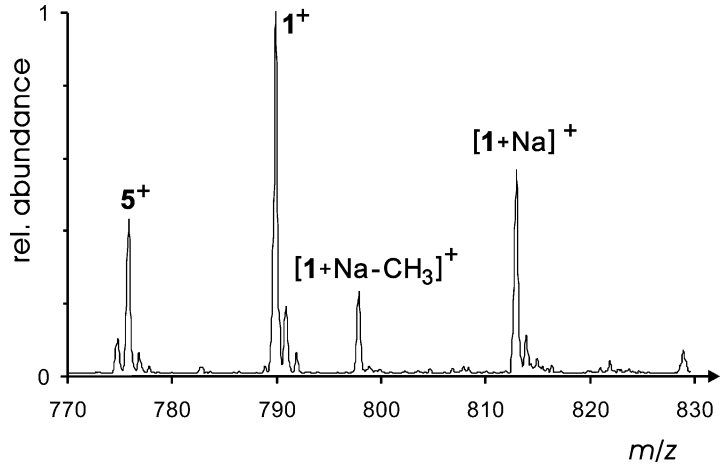

Fig. 1. Partial ESI spectrum (m/z = 770–830) of **1** dissolved in methanol under gentle ionization conditions (U_c = 15 V).

of methyl radicals ($\Delta m = -15n$ with n = 1–4). In addition, mass differences such as $\Delta m = -16$ (CH_4 or O), $\Delta m = -31$ ($CH_3^\bullet + CH_4$ or $CH_3O^\bullet$), and $\Delta m = -32$ (2 CH_4, CH_3OH, or O_2) are observed at high collision energies; note that also $\Delta m = -30$ not only represents the loss of two methyl radicals, but can also arise from the expulsion of CH_2O. In contrast, losses of $CH_3^\bullet$ are of minor abundance for the molecular ion $\mathbf{1}^+$ and the fragment $\mathbf{2}^+$, for which losses of neutral $OV(OCH_3)_3$ are clearly preferred. In the sequence $\mathbf{1}^+ \rightarrow \mathbf{2}^+ \rightarrow \mathbf{3}^+ \rightarrow \mathbf{4}^+$, the cluster formally expulses all vanadium(V) centers present in $\mathbf{1}^+$ as mononuclear $OV(OCH_3)_3$ units to finally reach the "pure" V_3^{IV} compound $\mathbf{4}^+$.

In order to explore the consecutive fragmentation behavior of ionized **1** in more detail, mass-selected $\mathbf{1}^+$–$\mathbf{4}^+$ were subjected to CID experiments at various collision energies (Table 1). Upon CID of the molecular ion $\mathbf{1}^+$ with xenon as the collision gas, $\mathbf{2}^+$ appears as the first fragment. Gradual increase of the collision energy affords $\mathbf{3}^+$ from which consecutive $CH_3^\bullet$ losses occur at even larger collision energies (Fig. 2). Further, loss of $OV(OCH_3)_3$ to generate the trivanadium cluster $V_3O_4(OCH_3)_3^+$ ($\mathbf{4}^+$), is observed at elevated collision energies. These observations tentatively suggest the fragmentation pathways shown in Scheme 1.

Thus, energized $\mathbf{1}^+$ consecutively expels two $OV(OCH_3)_3$ units to first afford $\mathbf{2}^+$ and then $\mathbf{3}^+$; in the following, such a loss of vanadium from the ionic species is referred to as "cluster degradation." This is contrasted by loss of outer CH_3 substituents from tetranuclear $\mathbf{3}^+$, although the expulsion of another $OV(OCH_3)_3$ unit to yield $\mathbf{4}^+$ can compete. Note that the loss of CH_3 units is associated with an increase of the formal oxidation state of the cluster, e.g., $V_3^{IV}V^V$ in $\mathbf{3}^+$ changes to $V_2^{IV}V_2^V$ in $[\mathbf{3} - CH_3]^+$. The series of $CH_3^\bullet$ losses yields intense fragment ions down to $V_4O_9(OCH_3)_2^+$ (m/z = 410), a formal $V_4^{V+\bullet}$ radical cation which is the last member of this series.

This fragmentation scheme is fully supported by the CID spectra of mass-selected $\mathbf{2}^+$ and $\mathbf{3}^+$, respectively (Table 1). Thus, CID of $\mathbf{2}^+$ affords $\mathbf{3}^+$ as the first product, and CID of mass-selected $\mathbf{3}^+$ confirms the competition of $CH_3^\bullet$ and $OV(OCH_3)_3$ losses from the tetranuclear cluster ion. In continuation of the trend from exclusive cluster degradation for $\mathbf{1}^+$ and $\mathbf{2}^+$, competition of cluster degradation and losses of outer substituents from $\mathbf{3}^+$, CID of mass-selected $\mathbf{4}^+$ does not show a notable extent of cluster degradation. Instead, $\mathbf{4}^+$ undergoes sequential losses of outer substituents mostly leading to the $V_3O_5^+$ cation (m/z = 233), a formal $V^{III}V_2^{IV}$ compound (Fig. 3).

Table 1
Major fragments[a] (given as mass differences Δm) in the low-energy CID mass spectra of mass-selected cluster ions generated by ESI of neutral **1** dissolved in methanol at variable collision energies (E_{lab} in eV)

	E_{lab}	M^{+}[b]	−15	−30	−32	−160	−175	−192	−320	−352
$\mathbf{1}^{+}$	5	100				10			4	
	10	100				35			20	
	20	20				35			100	
2	5	100				65	1		1	
	10	8				100	4		3	
	20					65	60		100	
$\mathbf{3}^{+}$	5	100	8	2		8	1			
	10	100	60	15		70	15			
	20[c]	5	10	15		60	100			
$\mathbf{4}^{+}$[d]	5	100	35	4						
	10	25	100	20						
	20[e]	3	8	10						
$\mathbf{5}^{+}$	5	100			20					
	10	40			100			15		10
	20	5			30			35		100

[a] Relative intensities normalized to the base peak (100).
[b] Intensity of the mass-selected parent ion M^{+} relative to the base peak.
[c] Additional losses of outer substituents not included.
[d] Another major fragmentation leads to $V_3O_5^{+}$ ($\Delta m = -77$, formally corresponding to losses of one CH_3 and two CH_3O units as neutrals) with relative intensities of 1, 6, and 100 at $E_{lab} = 5$, 10, and 20 eV, respectively (see text).
[e] The base peak (100) corresponds to $V_3O_5^{+}$ ($m/z = 233$), see footnote c and Fig. 3.

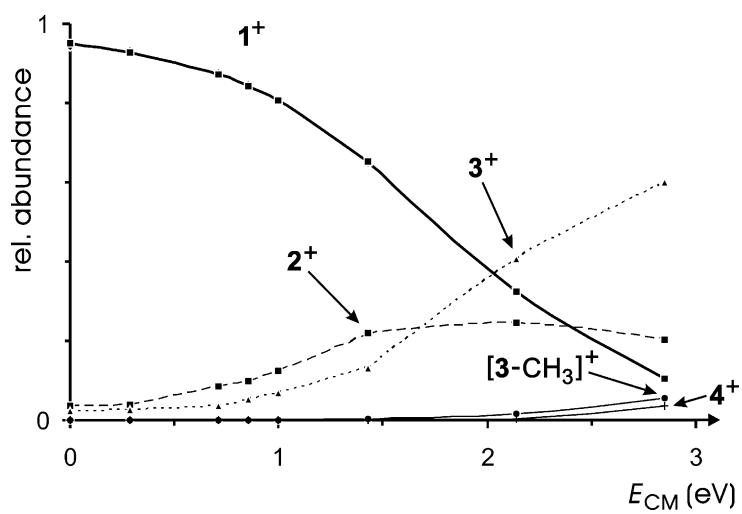

Fig. 2. Evolution of the major fragment ions upon CID of mass-selected $\mathbf{1}^{+}$ at collision energies up to $E_{CM} = 3$ eV; collision gas: xenon. Secondary fragmentations of $[\mathbf{3} - CH_3]^{+}$ and $\mathbf{4}^{+}$, respectively, were summed to these channels. The solid line for the parent ion is a fit with the sigmoid function discussed in the text.

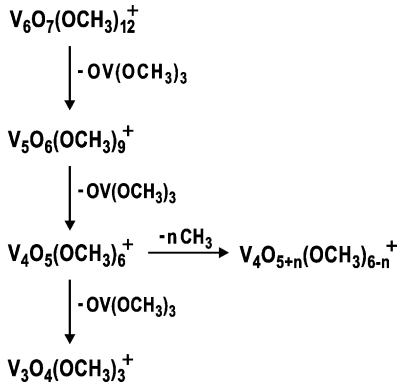

Scheme 1.

The molecular anion $\mathbf{1}^-$ is easily generated by ESI of a dilute solution of *n*-$C_4H_9N[V_6O_7(OCH_3)_{12}]$ in methanol. In fact, $\mathbf{1}^-$ is by and large the only signal in the negative ion ESI mass spectrum of this compound, if the ionization conditions are relatively mild (Fig. 4a). More harsh ionization induces fragmentation of the molecular ion $\mathbf{1}^-$, where again two consecutive losses of $OV(OCH_3)_3$ followed by expulsions of methyl radicals are observed (Fig. 4b). Quite remarkably, this fragmentation sequence of the anion, i.e., $\mathbf{1}^- \rightarrow \mathbf{2}^- \rightarrow \mathbf{3}^-$ and then losses of $CH_3^\bullet$ radicals, coincides with that of the cationic species $\mathbf{1}^+$, except that degradation to the trinuclear cluster anion $\mathbf{4}^-$ is hardly observed. CID of mass-selected $\mathbf{1}^-$ fully supports this analysis, although unusually large collision energies are required in order to induce notable dissociation of the anionic species. At a collision energy of $E_{lab} = 50$ eV, for example, no significant fragmentation of $\mathbf{1}^-$ is observed. With xenon as the collision gas, this value corresponds to a center-of-mass energy of $E_{CM} \approx 7$ eV. Only at about $E_{lab} = 70$ eV, and thus $E_{CM} \approx 10$ eV, notable fragmentation of $\mathbf{1}^-$ starts to occur affording $\mathbf{2}^-$ and $\mathbf{3}^-$, respectively. For the latter, losses of $CH_3^\bullet$ are preferred over further degradation of the tetranuclear cluster to $\mathbf{4}^-$. Again, the results are fully supported by CID experiments of mass-selected $\mathbf{2}^-$ and $\mathbf{3}^-$ (not shown). In addition, a loss of $\Delta m = -62$, presumably $CH_3OH + CH_2O$ formed in an internal disproportionation of two methoxy groups, is observed from $\mathbf{1}^-$, once more with consecutive losses of two $OV(OCH_3)_3$ units (each, $\Delta m = -160$) from the resulting fragment ion at elevated collision energies. Although the dissociation of large, covalently bound cluster ions might be subject to substantial kinetic shifts [8], the fragmentations of the various cationic species examined in this study require much lower collision energies. Instead of a particularly pronounced stability of the anionic cluster, we propose that fragmentation of $\mathbf{1}^-$ competes with electron detachment, $\mathbf{1}^- \rightarrow \mathbf{1} + e^-$. If the latter were

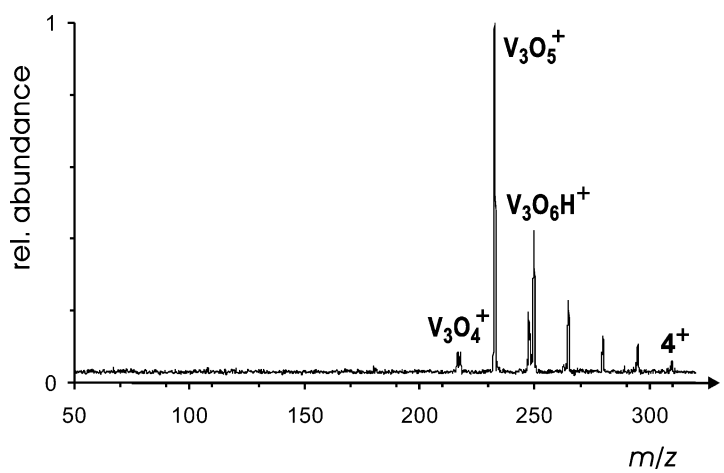

Fig. 3. Representative CID spectrum of mass-selected $\mathbf{4}^+$ generated at $U_c = 115$ V; collision gas: xenon, $E_{lab} = 20$ eV. The major fragment ions correspond to $m/z = 295$, 280, 265, 250 ($V_3O_6H^+$), 248, 233 ($V_3O_5^+$), and 217 ($V_3O_4^+$).

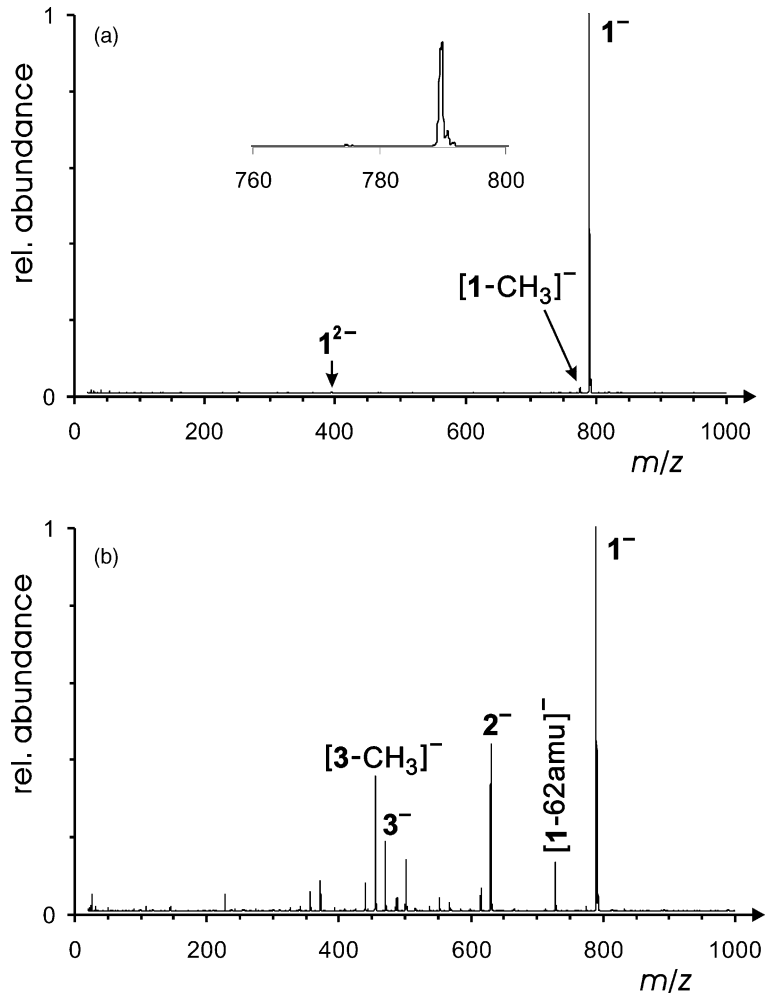

Fig. 4. ESI spectrum of $(n\text{-}C_4H_9)_4N[V_6O_7(OCH_3)_{12}]$ dissolved in methanol at (a) gentle ionization conditions ($U_c = 15$ V) and (b) elevated cone voltage ($U_c = 150$ V). Note that also a trace of the dianion $\mathbf{1}^{2-}$ is observed at low cone voltage.

energetically more favorable, it is easily understood that anionic fragments are only observed at large collision energies. Unfortunately, attempts to estimate the electron affinity of **1** by means of the kinetic method [9] were unsuccessful, because addition of various bases **B** (nitrophenols were employed) to the methanolic solution of $(n\text{-}C_4H_9)_4N[V_6O_7(OCH_3)_{12}]$ does not produce significant amounts of adducts of the type $[\mathbf{B}\cdot\mathbf{1}]^-$ which might have been used afterwards to estimate the electron affinity of **1** in MS/MS experiments. For the time being, we therefore cannot decide whether or not the anionic clusters are particularly stable or electron detachment is efficiently competing. Notwithstanding, it is to be pointed out that the observed fragmentation behavior of the anion is very similar to that of the cationic species.

For the cationic species, the results were further supported by partial labeling of **1**. To this end, a submolar aliquot of **1** was dissolved in 2 mL CD_3OD. The ESI spectrum of the freshly prepared sample of this solution is very similar to that shown in Fig. 1. After 4 days storage at room temperature, however, notable incorporation of deuterium is observed (Fig. 5). Nevertheless, the isotope pattern is far from statistical

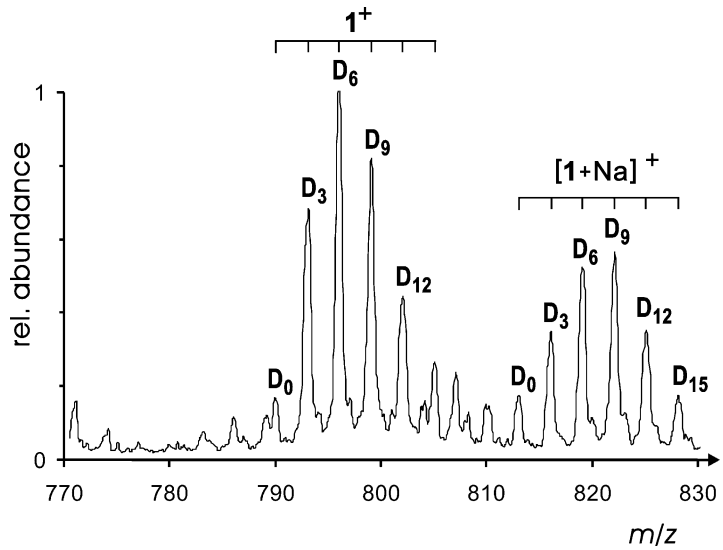

Fig. 5. Partial ESI spectrum (m/z = 770–830) of **1** dissolved in CD_3OD after 4 days storage at room temperature. Compared to Fig. 1, the patterns clearly show the incorporation of OCD_3 units into $\mathbf{1}^+$ as well as $[\mathbf{1} + Na]^+$ as indicated by the labels D_0–D_{15}.

deuteration in that mass differences of $\Delta m = 3$ prevail. Accordingly, we conclude that upon storage of the solution, neutral **1** has undergone degenerate methanolysis in which OCH_3 groups are sequentially exchanged by OCD_3 moieties to yield partially deuterated $V_6O_7(OCH_3)_{12-n}(OCD_3)_n$, and the corresponding molecular cations ($m/z = 790 + 3n$) with the maximum at $n = 2$ are formed upon ESI. The practical absence of intermediate labels, i.e., $\Delta m = 1$ or 2 (except of the expected ^{13}C contributions), indicates that the methoxy groups of **1** remained intact in methanolic solution. The similar pattern observed for the corresponding sodium adducts ($m/z = 813 + 3n$) fully supports this line of reasoning, although we cannot provide a straightforward explanation why the maximum of deuterium incorporation differs for the sodium adducts. Further insight into the ion chemistry is gained from inspection of the CID spectrum of mass-selected $V_6O_7(OCH_3)_9(OCD_3)_3{}^+$ (m/z = 799) at low collision energies (E_{lab} = 10 V) in which the first step of cluster degradation gives rise to a ca. 80:110:25:1 distribution of the pentanuclear ions $V_5O_6(OCH_3)_6(OCD_3)_3{}^+$ (m/z = 639), $V_5O_6(OCH_3)_7(OCD_3)_2{}^+$ (m/z = 636), $V_5O_6(OCH_3)_8(OCD_3)^+$ (m/z = 633), and $V_5O_6(OCH_3)_9{}^+$ (m/z = 630). Compared to the statistically expected pattern of 84:108:27:1 for the $V_5O_6(OCH_3)_{6+n}(OCD_3)_{3-n}{}^+$ fragments (n = 0–3), the rearrangement obviously required in cluster degradation appears to be associated with a negligible kinetic isotope effect. Further, the absence of intermediate signals rules out the occurrence of partial H/D exchange processes prior to dissociation. Both observations strongly suggest that the methoxy units remain intact upon cluster degradation, thereby disproving the occurrence of hidden hydrogen transfers [10] in possible redox processes prior to loss of $OV(OCH_3)_3$ from $\mathbf{1}^+$, which are otherwise well-known to occur in the gas-phase chemistry of transition metal alkoxides [11–15]. Likewise, only signals with m/z = 470, 473, 476, and 479 are observed for the corresponding tetranuclear fragment ions, $V_4O_5(OCH_3)_{6-n}(OCD_3)_n{}^+$ (n = 0–3).

3.2. H^+, Na^+, and Cs^+ adducts of **1**

In addition to the molecular ions, ESI also allows the generation of cationized **1**. Thus, ESI of a solution of **1** in methanol/water (50:50) with 1% formic acid provides a signal due to $[\mathbf{1} + H]^+$ with m/z =

791 (HR: $m_{exp} = 790.8556$, $m_{th} = 790.8567$, $\Delta m = 0.0011$); without the addition of formic acid, the signal at $m/z = 791$ is mostly due to ^{13}C-**1**$^+$ instead of $[\mathbf{1} + H]^+$ (see above). CID of mass-selected $[\mathbf{1} + H]^+$ shows first loss of methanol ($\Delta m = -32$) and then two sequential losses of $OV(OCH_3)_3$ ($\Delta m = -160$), and finally a series $CH_3^\bullet$ expulsions ($\Delta m = -15$), that is the sequence: $791 \rightarrow 759 \rightarrow 599 \rightarrow 439 \rightarrow [439 - 15n]$ (Table 2). Thus, the protonated species also behaves similarly to the molecular ions **1**$^+$ and **1**$^-$, except that loss of methanol occurs as the first step.

Even closer is the analogy of the molecular ion **1**$^+$ with the behavior of the sodium adduct $[\mathbf{1}+Na]^+$ with $m/z = 813$ (HR: $m_{exp} = 812.8374$, $m_{th} = 812.8386$, $\Delta m = 0.0012$) which is co-generated upon ESI of **1** in methanol due to traces of sodium present in the sample (Fig. 1). CID of mass-selected $[\mathbf{1} + Na]^+$ shows the very same sequence observed for **1**$^+$ and **1**$^-$, i.e., $[\mathbf{1} + Na]^+ \rightarrow [\mathbf{2} + Na]^+ \rightarrow [\mathbf{3} + Na]^+$ and then prevailing losses of $CH_3^\bullet$. At large collision energies, the expulsion of another $OV(OCH_3)_3$ unit to form $[\mathbf{4} + Na]^+$ ($m/z = 333$) is observed. Again, the fragmentation scheme is fully supported by the CID studies of the mass-selected fragment ions generated at elevated cone voltages (Table 2). Interestingly, the signal of mass-selected $[\mathbf{4}+Na]^+$ disappears upon CID without any intense fragment ions being formed. Careful examination of the low-mass region reveals that this ion undergoes loss of neutral **4**. While the corresponding Na^+ fragment was observed experimentally, it is expected to be subject to a substantial mass discrimination, in particular when using xenon as the collision gas. Therefore, these results are not analyzed any

Table 2
Major fragments[a] (given as mass differences Δm) in the low-energy CID mass spectra of mass-selected cluster ions generated by ESI of neutral **1** dissolved in methanol at variable collision energies (E_{lab} in eV)

	E_{lab}	M$^+$[b]	−15	−30	−32	−160	−175	−192	−320	−352	−790
$[\mathbf{1} + H]^+$[c]	5	100			40						
	10	35			100			30			
	20	5			15			100		65	
$[\mathbf{1} + Na]^+$	5	100				4			2		
	10	100				8			7		
	20	90				40			100		
$[\mathbf{2} + Na]^+$	5	100				50	1				
	10	25				100	6		2		
	20	1				100	80		40		
$[\mathbf{3} + Na]^+$[d]	5	100	10	1		4					
	10	100	85	10		50	3				
	20	25	30	25		100	20				
$[\mathbf{4} + Na]^+$[e]	10	100	8								
$[\mathbf{1} + Cs]^+$[f]	5	100									1
	10	100									10
	20	30									100

[a] Relative intensities normalized to the base peak (100).
[b] Intensity of the mass-selected parent ion M$^+$ relative to the base peak.
[c] ESI solvent: CH_3OH/H_2O (50:50) with 1% HCOOH.
[d] Another major fragmentation leads to $NaV_3O_4(OCH_3)_4^+$ ($m/z = 364$; $\Delta m = -129$ corresponding to loss of $OV(OCH_3)_2$, rather than $OV(OCH_3)_3$) with relative intensities of 2, 40, and 75 at $E_{lab} = 5$, 10, and 20 eV, respectively.
[e] At elevated collision energies, the parent ion rapidly disappears while no intense fragment ions are observed, which is ascribed to the loss of the entire ligand **4** ($\Delta m = -310$) from the sodium cluster, see text.
[f] ESI solvent: CsCl-doped methanol.

further, except stating that in the case of $[\mathbf{4} + Na]^+$, the binding energy of sodium ion to the neutral cluster **4** appears to be significantly lower than the energy required for further fragmentation of the cluster itself.

Addition of a trace of CsCl to the methanolic solution of **1** provides an intense signal corresponding to $[\mathbf{1} + Cs]^+$ with $m/z = 923$. Upon CID, however, loss of the entire vanadium cluster, rather than consecutive degradation is observed. In fact, atomic Cs^+ is the only notable cationic fragment formed from $[\mathbf{1}+Cs]^+$ in the range of collision energies examined. Likewise, signals corresponding to $[\mathbf{2} + Cs]^+$, $[\mathbf{3} + Cs]^+$, or their fragments do not appear in ESI mass spectra of a CsCl-doped methanolic solution of **1** at elevated cone voltages. Accordingly, we conclude that the binding energy of Cs^+ to **1** is lower than the energy demand of cluster degradation in $[\mathbf{1} + Cs]^+$. With regard to analytical aspects, we note in passing that the clean generation of $[\mathbf{1} + Cs]^+$ upon ESI with CsCl-doped methanol nicely confirms the identity of the sample as genuine **1**.

3.3. Miscellaneous

In addition to $\mathbf{1}^+$, ESI of the $V_6O_7(OCH_3)_{12}$ sample gave rise to a signal at $m/z = 776$ (Fig. 1). Tentatively, we attribute this ion to a partial hydrolysis of **1** with residual water upon sample preparation to yield the monohydroxy cluster $V_6O_7(OCH_3)_{11}(OH)$ (**5**), and thus the corresponding molecular ion $\mathbf{5}^+$ upon ESI. This assignment is supported by (i) high-resolution mass spectra ($m_{exp} = 775.8345$, $m_{th} = 775.8332$, $\Delta m = -0.0013$), (ii) the increase of this signal upon addition of water to a methanolic solution of **1**, and (iii) the fragmentation behavior of mass-selected $m/z = 776$. Thus, CID of mass-selected $\mathbf{5}^+$ affords initial loss of methanol ($\Delta m = -32$), then two expulsions of $OV(OCH_3)_3$ ($\Delta m = -160$, each), again followed by loss of $CH_3^\bullet$ entities from the tetranuclear cluster; the corresponding fragmentation sequence is $776 \rightarrow 744 \rightarrow 584 \rightarrow 424 \rightarrow [424 - 15n]$ (Table 1). After initial loss of methanol, the modified cluster $\mathbf{5}^+$ thus obeys the same fragmentation scheme as $\mathbf{1}^+$. The fact that loss of methanol from $\mathbf{5}^+$ precedes that of $OV(OCH_3)_3$ implies that the activation barrier associated with proton transfer between the substituents is smaller than that associated with the complex rearrangements required in cluster degradation en route to the expulsion of $OV(OCH_3)_3$. Note that the analog reasoning applies for loss of methanol from $[\mathbf{1} + H]^+$ described above.

Formation of $\mathbf{5}^+$ by partial hydrolysis of **1** in solution is further supported by the observation of ions with $m/z = 762$, formally $V_6O_7(OCH_3)_{10}(OH)_2{}^+$, and $m/z = 748$, formally $V_6O_7(OCH_3)_9(OH)_3{}^+$, in the ESI mass spectrum of **1** dissolved in methanol/water (50:50). Upon CID of mass-selected $m/z = 762$, initial losses of either H_2O or CH_3OH are observed, where loss of H_2O prevails at low collision energies. At elevated cone voltages, these primary fragmentation are again followed by degradations to the corresponding penta- and tetranuclear clusters via sequential losses of $OV(OCH_3)_3$.

Further, some dimers were observed under mild ESI conditions, e.g., $[(\mathbf{1})_2]^+$ with $m/z = 1580$, $[(\mathbf{1})_2H]^+$ with $m/z = 1581$, $[(\mathbf{1})_2Na]^+$ with $m/z = 1603$ (HR: $m_{exp} = 1602.6870$, $m_{th} = 1602.6875$, $\Delta m = 0.0005$), and $[(\mathbf{1})_2Cs]^+$ with $m/z = 1713$. Because CID yields the corresponding monomers, these ions are considered as loosely bound dimers and not pursued any further.

3.4. CID breakdown behavior

The QHQ configuration of the VG BIO-Q mass spectrometer also allows to investigate the energy behavior of the ion fragmentations. Thus, CID experiments with mass-selected ions at various collision energies allude to the dependence of the fragmentations observed from the internal energy of the dissociating ions. Above, the variations of the fragment abundances as a function of collision energy were only discussed phenomenologically. In this section, these dependencies are expressed in breakdown diagrams of which the one of $\mathbf{1}^+$ is already shown in Fig. 2. The experimental data points can be fitted quite reasonably with sigmoid functions of the type $I_i(E_{CM}) = 1/(1 + e^{(E_{1/2}-E_{CM})b})$ by analogy to the

corresponding treatment of reaction efficiencies by Bouchoux et al. [16]; an example of such a fit is shown by the solid line for the parent ion $\mathbf{1}^+$ in Fig. 2. Within this framework, the breakdown curve is defined by two parameters: $E_{1/2}$ is the energy at which the sigmoid function has reached half of its maximum and the term b reflects the steepness of the sigmoid curve. As expressed here, the larger b, the steeper is the rise and the curve becomes a step function for $b \rightarrow \infty$.

The evaluation of the energy-dependent CID experiments fully confirms the qualitative conclusions derived above (Table 3). Consider the consecutive fragmentation of $\mathbf{1}^+$ as an example. For the primary dissociation, $\mathbf{1}^+ \rightarrow \mathbf{2}^+ + OV(OCH_3)_3$, the characteristic energy $E_{1/2} = 1.8\,eV$ is significantly larger than $E_{1/2} = 1.0\,eV$ for the next step, $\mathbf{2}^+ \rightarrow \mathbf{3}^+ + OV(OCH_3)_3$. This ordering is fully consistent with the fact that $\mathbf{2}^+$ never is the base peak in the CID spectra of $\mathbf{1}^+$ at variable collision energies. For the fragment $\mathbf{3}^+$, loss of an outer CH_3 substituent ($E_{1/2}(–CH_3) = 1.7\,eV$) is more facile than cluster degradation ($E_{1/2}(–OV(OCH_3)_3) = 2.1\,eV$), consistent with the fragmentation of mass-selected $\mathbf{1}^+$–$\mathbf{3}^+$ as well as the evolution of the ESI mass spectra with increasing cone voltages.

While the breakdown graphs (e.g., Fig. 2) do certainly contain information about the thermochemical thresholds of the associated fragmentations, we deliberately refrain from the extraction of exact thermodynamic quantities and only list the phenomenological appearance energies (AEs) corresponding to the onset of the respective fragmentations as derived from linear extrapolation of the rise at $E_{1/2}$ to the baseline. Apart from others, the most severe limitation which hinders us from a conversion to thermochemical thresholds is associated with the fact that most of the ions examined here were generated at elevated cone voltages. Thus, even though the ions initially generated upon ESI are

Table 3
Energy behavior of the breakdown curves in the low-energy CID mass spectra of mass-selected methoxo-oxovanadium cluster ions generated by ESI of neutral **1** dissolved in methanol[a]

	m/z	Lost neutral	U_c[b]	$E_{1/2}$[c,d]	b[c,d]	AE[e]
$\mathbf{1}^+$	790	$OV(OCH_3)_3$	50	1.8	2.0	0.8
$\mathbf{2}^+$	630	$OV(OCH_3)_3$	75	1.0	3.8	0.5
$\mathbf{3}^+$	470	$OV(OCH_3)_3$	90	2.1	2.3	1.3
		CH_3	90	1.7	2.7	0.9
$\mathbf{4}^+$	310	CH_3	115	1.8	2.5	1.0
$\mathbf{5}^+$[f]	776	CH_3OH	55	0.9	3.0	0.3
$[\mathbf{1} + H]^+$[g]	791	CH_3OH	45	1.0	4.0	0.5
$[\mathbf{1} + Na]^+$	813	$OV(OCH_3)_3$	70	1.7	2.5	1.2
$[\mathbf{2} + Na]^+$	653	$OV(OCH_3)_3$	90	1.2	3.0	0.6
$[\mathbf{3} + Na]^+$	493	$OV(OCH_3)_3$	110	1.8	3.0	1.1
		CH_3	110	1.8	2.5	1.0
$[\mathbf{1} + Cs]^+$[h]	923	**1**	15	2.12[i]	3.3	1.48[i]
			45	2.06[i]	3.2	1.42[i]
			75	2.01[i]	2.6	1.23[i]

[a] Energy behavior fitted to a sigmoid function with the parameters $E_{1/2}$ and b, where $E_{1/2}$ refers to the collision energy in the center-of-mass frame (see text).
[b] Cone voltage (U_c in V) at which maximal abundance of the ion of interest was achieved.
[c] See text for a description of the parameters $E_{1/2}$ (in eV) and b (in eV^{-1}).
[d] Error bars: $\pm 0.05\,eV$ for $E_{1/2}$ and $\pm 0.10\,eV^{-1}$ for b.
[e] Appearance energy (in eV) derived from extrapolation of the linear rise of the sigmoid function at $E_{1/2}$ to the onset of fragmentation.
[f] ESI solvent: methanol/water (50:50).
[g] ESI solvent: methanol/water/HCCOH (50:50:1).
[h] ESI solvent: CsCl doped methanol.
[i] Here, $E_{1/2}$ and AE are given with three figures significant for the comparison of the relative energetics at different cone voltages, see text.

assumed to be equilibrated to the source temperature (here 80–120 °C), the ions produced upon multicollisional dissociation in the cone region do not undergo further stabilization and thus have unknown distributions of internal energies, most likely corresponding to higher effective temperatures. To explicitly probe this effect, CID breakdown curves of mass-selected $[\mathbf{1} + Cs]^+$ were recorded at different cone voltages (last three entries in Table 3). As expected, both $E_{1/2}$ and b as well as the appearance energies decrease with increasing cone voltage. Thus, the higher the cone voltage, the more energized is the population of mass-selected $[\mathbf{1} + Cs]^+$. For this particular ion, extrapolation to thermal conditions (i.e., $U_c = 0$ V) suggest AE $= 1.5 \pm 0.1$ eV for the loss of neutral **1** from $[\mathbf{1} + Cs]^+$ affording bare Cs^+. For most of the other cluster ions, however, such an extrapolation is impossible because these are only formed at elevated cone voltages. Moreover, the cone voltage does not represent an independent parameter which could easily be incorporated in terms of an empirical modeling. Instead, the cone voltage at which best yields of a certain fragment ion are achieved depends on the stabilities of the predecessors and their subsequent dissociation products. If additional information were available, e.g., accurate ab initio data, these cooperative effects might be acknowledged by modeling the curves with explicit consideration of internal energy effects and the relevant dissociation thresholds. For transition metal clusters of the size of **1**, however, ion thermalization prior to energy-resolved CID experiments is not only advantageous, but a prerequisite for a more elaborate investigation of the ions' thermochemistry.

3.5. Excessive fragmentation of **1** upon ESI

At high cone voltages, the parent ions of each series, i.e., $\mathbf{1}^+$, $[\mathbf{1}+H]^+$, $[\mathbf{1}+Na]^+$, and $\mathbf{5}^+$ have almost disappeared while rich patterns of cluster ions are observed. Consistent with the fragmentation schemes outlined above, the resulting spectra are dominated by tri- and tetranuclear cluster ions. Depending on the ESI conditions and the composition of the solvent, the distributions of the cations can be changed from prevailing sodium adducts to oxovanadium-alkoxide clusters or almost pure $V_mO_n^+$ ions ($m = 1$–4, $n = 0$–10); an example is given in Fig. 6. Likewise, ESI of $(n\text{-}C_4H_9)_4N[V_6O_7(OCH_3)_{12}]$ at high cone voltages can be used for the generation of $V_mO_n^-$ ions ($m = 1$–4, $n = 3$–11). While it is beyond the scope of this paper to deeply analyze these cluster-ion distributions, a more general perspective is addressed

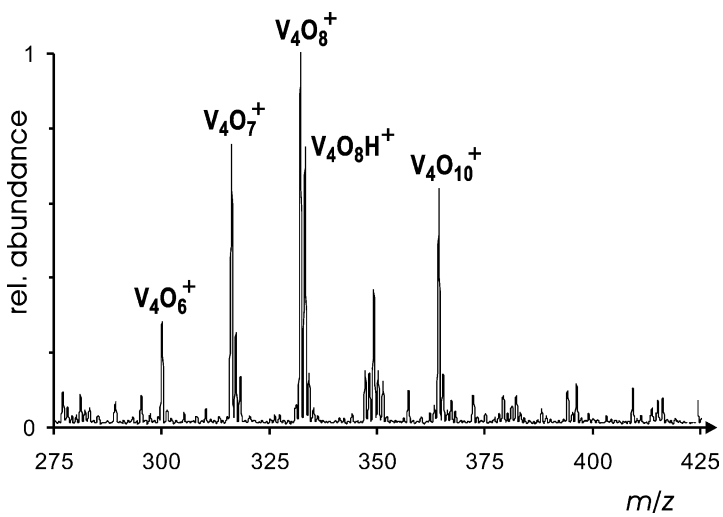

Fig. 6. ESI spectrum of **1** dissolved in methanol/water (50:50) at $U_c = 180$ V.

here. In particular, the relatively broad distributions of still reasonably intense cluster ions combined with the scanning modes possible in a QHQ device permit a rapid screening of the reactivities of these clusters in a straightforward manner.

With respect to the relevance of vanadium-oxide catalysts in the partial oxidation of C_4-hydrocarbons to maleic anhydride [17], *n*-butane was chosen as a simple test substrate in preliminary reactivity studies using various scan modes. The first approach employs a Q2 scan in which Q1 is set on full transmission while the hexapole is set to $E_{lab} = 0$ V and filled with ca. 10^{-3} mbar butane. In comparison with the same spectrum recorded in the absence of butane, such a scan can provide an overview of the ion reactivities: ions which react with *n*-butane decrease in abundance, while the ionic products formed in these reactions gain in abundance. Because the differences are only gradual, the corresponding difference spectrum is more sensitive. Among others, the signals at $m/z = 332$ and 364 give rise to negative signals in the difference spectrum, while inter alia $m/z = 390$ and 422 appear on the positive scale (Fig. 7a).

While it is difficult to deduce the occurrence of certain reactions from such a difference spectrum, it readily identifies those ions which are at all capable of reacting with butane. A more specific analysis can then be performed by conventional MS/MS techniques. As an example, the reaction of mass-selected $m/z = 332$ ($V_4O_8^+$ according to HR: $m_{exp} = 331.7359$, $m_{th} = 331.7352$, $\Delta m = -0.0007$; IRMPD) with butane is shown in Fig. 7b, where a formal addition of the butane unit to the cluster ion is observed ($m/z = 332 \rightarrow m/z = 390$); the additional signal at $m/z = 350$ is attributed to the association of $V_4O_8^+$ with water present in the background. We note in passing that Castleman and coworkers found that $V_4O_8^+$ generated by the laser-evaporation method were unreactive towards *n*-butane [18]; a possible explanation is the generation of isomeric cluster ions in the different methods used for ion generation [1,3,4]. With a neutral-gain spectrum, which is a simultaneous scan of both analyzers Q1 and Q2 with a constant mass difference (Δm_N) between them, in the next step, all ions which add butane can be probed when Δm_N is set to +58 (Fig. 7c). Likewise, neutral-gain and neutral-loss spectra can be used to identify those cluster ions which are capable to dehydrogenate butane ($\Delta m_N = +2$ or +56) or promote oxygen-atom transfer ($\Delta m_N = -16$); in these respects, the ion at $m/z = 364$ is particularly reactive. Further, comparison with the corresponding mass spectra in the absence of the reagent gas allows to estimate the relative reaction efficiencies for those ions.

For the time being, we will not dwell upon the details of these reactions because several obstacles need to be resolved. For example, the particularly interesting reactions of the ion with $m/z = 364$ (dehydrogenation and O-atom transfer) can be attributed to at least three different isobaric components: (i) the pure vanadium-oxide cluster $V_4O_{10}^+$ which may be formed upon consecutive dissociation of $\mathbf{3}^+$, (ii) the oxovanadium-methoxide cluster $V_4O_7(OCH_3)(OH)^+$ accessible from $\mathbf{5}^+$, and (iii) the sodiated cluster $NaV_3O_4(OCH_3)_4^+$ generated from $[\mathbf{3} + Na]^+$ upon loss of $OV(OCH_3)_2$. Under FT-ICR conditions in the Apex III, only the latter two ions could clearly be identified, whereas $V_4O_{10}^+$ was not observed; the ratio between $V_4O_7(OCH_3)(OH)^+$ (HR: $m_{exp} = 363.7628$, $m_{th} = 363.7608$, $\Delta m = -0.0020$; IRMPD) and $NaV_3O_4(OCH_3)_4^+$ (HR: $m_{exp} = 363.8762$, $m_{th} = 363.8743$, $\Delta m = -0.0019$; IRMPD) strongly depended on experimental conditions. In the VG BIO-Q, however, more extensive fragmentation in the cone region is observed and the relatively clean $V_nO_m^+$ patterns (e.g., Fig. 6) might suggest that also $V_4O_{10}^+$ is formed under these conditions. Notwithstanding these difficulties in the identification of the reactive components, it is pointed out that ESI of well-defined molecular precursors may provide an alternative method for the generation of vanadium-oxide cluster ions in the gas phase. Moreover, combination with the various scanning modes possible in a multipole device provides a means to screen the bimolecular reactivities of a wide set of cluster ions at thermal energies.

Finally, we note in passing that none of the various anionic clusters accessible from ESI of $(n\text{-}C_4H_9)_4N[V_6O_7(OCH_3)_{12}]$ at elevated cone voltages showed

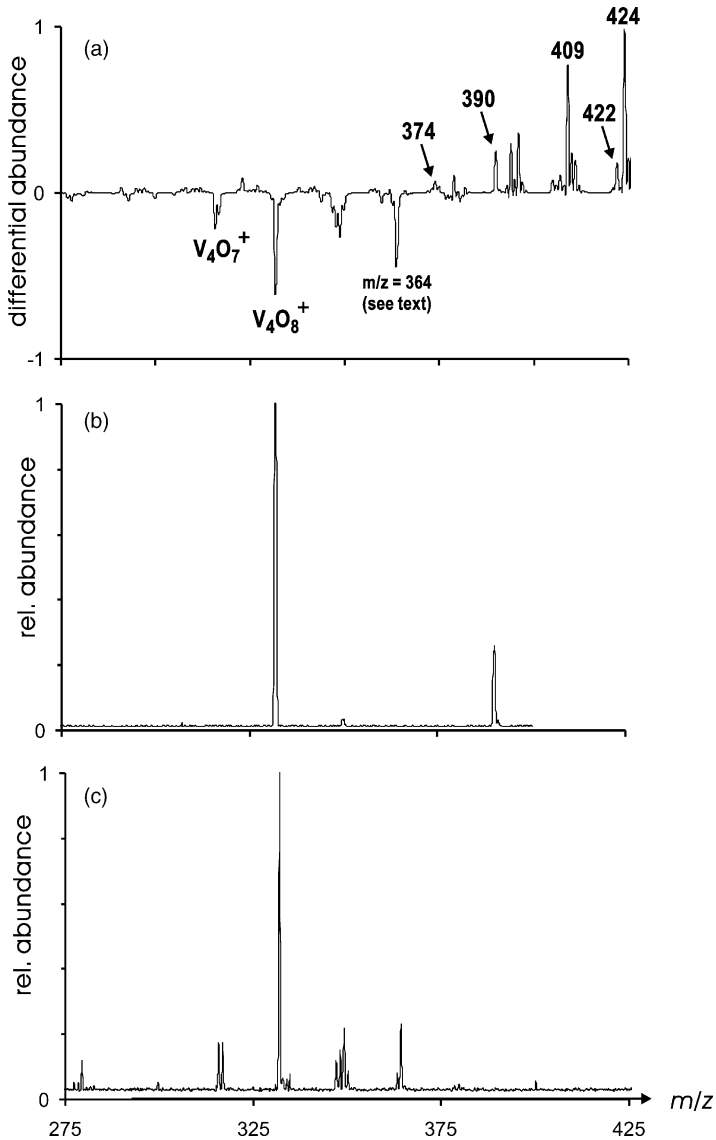

Fig. 7. (a) Difference of the ESI spectra (Q2 scan; $m/z = 275$–425) of **1** at $U_c = 180$ V in the presence and the absence of butane in the hexapole ($E_{lab} = 0$ V). The positive signals for $m/z = 409$ and 424 can be attributed to CID of larger cluster ions under these conditions. (b) Q2 scan ($m/z = 275$–425) of the products formed in the reaction of Q1-selected $m/z = 332$ with butane present in the hexapole ($E_{lab} = 0$ V). (c) Neutral-gain scan ($\Delta m = +58$) of the region from $m/z = 275$ to $m/z = 425$ with butane present in the hexapole ($E_{lab} = 0$ V).

any notable reactivity towards butane. The lack of reactivity of the $V_mO_n^-$ cluster anions with *n*-butane parallels our previous, more general considerations on the bond activation of hydrocarbons by small transition metal anions in the gas phase [19].

4. Conclusions

Anionic and cationic $\mathbf{1}^{-/+}$ by and large show the same type of fragmentation behavior. Two initial losses of $OV(OCH_3)_3$ afford the corresponding

tetranuclear cluster ion $\mathbf{3}^{-/+}$, from which losses of outer substituents, preferentially CH_3 groups, prevail at elevated energies; loss of another $OV(OCH_3)_3$ unit is less favorable. Because we may further assume quite safely that the positive charge in $[\mathbf{1} + Na]^+$ is mostly located on the alkaline metal, the more or less identical fragmentation behavior of the Na^+ adduct can therefore be assigned to reflect the dissociation of neutral **1**, where the sodium just serves the function to keep the cluster charged. Accordingly, the fragmentation scheme $\mathbf{1} \rightarrow \mathbf{2} \rightarrow \mathbf{3}$ with subsequent losses of outer substituents is considered as an intrinsic property of the $V_6O_7(OCH_3)_{12}$ cluster irrespective of the actual charge state. The situation changes once active protons are present in the cluster in that loss of methanol becomes much more favorable than cluster degradation. The resulting fragments, however, again display the characteristic pattern: first, two losses of $OV(OCH_3)_3$ and then expulsions of CH_3 groups.

The ESI mass spectra acquired under more drastic ionization conditions demonstrate that well-defined molecular clusters such as **1** can serve as versatile precursors for the generation of cluster ions in the gas phase, thereby complementing the widespread application of laser-evaporation techniques. Particularly remarkable is the facile tuning of the cluster distributions by variation of the ESI conditions. Hence, molecular clusters can be used as alternative means in reactivity studies of heteronuclear transition metal cluster ions.

Acknowledgements

This work was supported by the Deutsche Forschungsgemeinschaft and the Sonderforschungsbereich 546.

References

[1] K.R. Asmis, M. Brümmer, C. Kaposta, G. Santambrogio, G. van Helden, G. Meijer, K. Rademann, L. Wöste, Phys. Chem. Chem. Phys. 4 (2002) 1101.
[2] S.F. Vyboishchikov, J. Sauer, J. Phys. Chem. A 105 (2001) 8588.
[3] H. Wu, S.R. Desai, L.S. Wang, J. Am. Chem. Soc. 118 (1995) 5296.
[4] H. Wu, L.S. Wang, J. Chem. Phys. 108 (1998) 5310.
[5] J. Spandl, I. Brügdam, H. Hartl, Z. Anorg. Allg. Chem. 626 (2000) 2125.
[6] J. Spandl, C. Daniel, I. Brügdam, H. Hartl, Angew. Chem. 115 (2003) 1195;
J. Spandl, C. Daniel, I. Brügdam, H. Hartl, Angew. Chem. Int. Ed. 42 (2003) 1163.
[7] D. Schröder, T. Weiske, H. Schwarz, Int. J. Mass Spectrom. 219 (2002) 759.
[8] J. Laskin, C. Lifshitz, J. Mass Spectrom. 36 (2001) 459.
[9] R.G. Cooks, P.S.H. Wong, Acc. Chem. Res. 31 (1998) 379.
[10] H. Schwarz, Top. Curr. Chem. 97 (1981) 1.
[11] M.B. Wise, D.B. Jacobson, B.S. Freiser, J. Am. Chem. Soc. 107 (1985) 1590 and 6744.
[12] D. Schröder, H. Schwarz, Angew. Chem. 102 (1990) 925;
D. Schröder, H. Schwarz, Angew. Chem. Int. Ed. Engl. 29 (1990) 910.
[13] A. Fiedler, D. Schröder, H. Schwarz, B.L. Tjelta, P.B. Armentrout, J. Am. Chem. Soc. 118 (1996) 5047.
[14] S. Géribaldi, S. Breton, M. Decouzon, M. Azzaro, J. Am. Soc. Mass Spectrom. 7 (1996) 1151.
[15] T. Waters, R.A. O'Hair, A.G. Wedd, Chem. Commun. (2000) 225.
[16] G. Bouchoux, D. Leblanc, M. Sablier, Int. J. Mass Spectrom. 210/211 (2001) 189, and references cited therein.
[17] B. Chen, E.J. Munson, J. Am. Chem. Soc. 124 (2002) 1638, and references cited therein.
[18] R.C. Bell, K.A. Zemski, K.P. Kerms, H.T. Deng, A.W. Castleman Jr., J. Phys. Chem. A 102 (1998) 1733.
[19] D. Schröder, H. Schwarz, S. Shaik, in: B. Meunier (Ed.), Metal-Oxo and Metal-Peroxo Species in Catalytic Oxidations, Struct. Bond., vol. 97, Springer, Berlin, 2000, p. 91.